


<b>ITC 4/51</b> Information Technology and Control Vol. 51/ No. 4 / 2022 pp. 786-800 DOI 10.5755/j01.itc.51.4.28052	<b>Alzheimer's Disease Segmentation and Classification on MRI Brain          Images Using Enhanced Expectation Maximization Adaptive Histogram          (EEM-AH) and Machine Learning</b>	
	Received 2020/11/22	Accepted after revision 2021/03/11
	 <a href="http://dx.doi.org/10.5755/j01.itc.51.4.28052">http://dx.doi.org/10.5755/j01.itc.51.4.28052</a>	

**HOW TO CITE:** Ramya, J., Uma Maheswari, B., Rajakumar, M.P., Sonia, R. (2022). Alzheimer's Disease Segmentation and Classification on MRI Brain Images Using Enhanced Expectation Maximization Adaptive Histogram (EEM-AH) and Machine Learning. *Information Technology and Control*, 51(4), 786-800. <http://dx.doi.org/10.5755/j01.itc.51.4.28052>

# Alzheimer's Disease Segmentation and Classification on MRI Brain Images Using Enhanced Expectation Maximization Adaptive Histogram (EEM-AH) and Machine Learning

## J. Ramya

Department of Computer Science and Engineering; St. Joseph's College of Engineering; OMR, Chennai- 600 119, Tamilnadu, India; phone: 94866 25358; e-mail: ramsharsha@gmail.com

## B. Uma Maheswari

Department of Computer Science and Engineering; St. Joseph's College of Engineering; OMR, Chennai- 600 119, Tamilnadu, India; phone: 99400 91240; e-mail: mahespal2002@gmail.com

## M.P. Rajakumar

Department of Computer Science and Engineering; St. Joseph's College of Engineering; OMR, Chennai- 600 119, Tamilnadu, India; phone: 94440 65025; e-mail: rajranjhu@gmail.com

## R. Sonia

B. S. Abdur Rahman Crescent Institute of Science and Technology Chennai- 600 048, Tamilnadu, India; e-mail: sonia.j25@gmail.com

---

**Corresponding author:** ramsharsha@gmail.com

---

Alzheimer's disease (AD) is an irreversible ailment. This ailment causes rapid loss of memory and behavioral changes. Recently, this disorder is very common among the elderly. Although there is no specific treatment for this disorder, its diagnosis aids in delaying the spread of the disease. Therefore, in the past few years, automatic recognition of AD using image processing techniques has achieved much attraction. In this research, we propose a novel framework for the classification of AD using magnetic resonance imaging (MRI) data. Initially, the image is filtered using 2D Adaptive Bilateral Filter (2D-ABF). The denoised image is then enhanced using Entropy-based Contrast Limited Adaptive Histogram Equalization (ECLAHE) algorithm. From enhanced data, the region of interest (ROI) is segmented using clustering and thresholding techniques. Clustering is performed using Enhanced Expectation Maximization (EEM) and thresholding is performed using Adaptive Histogram (AH) thresholding algorithm. From the ROI, Gray Level Co-Occurrence Matrix (GLCM) features are generated. GLCM is a feature that computes the occurrence of pixel pairs in specific spatial coordinates of an image. The dimension of these features is reduced using Principle Component Analysis (PCA). Finally, the obtained features are classified using classifiers. In this work, we have employed Logistic Regression (LR) for classification. The classification results were achieved with the accuracy of 96.92% from the confusion matrix to identify the Alzheimer's Disease. The proposed framework was then evaluated using performance evaluation metrics like accuracy, sensitivity, F-score, precision and specificity that were arrived from the confusion matrix. Our study demonstrates that the proposed Alzheimer's disease detection model outperforms other models proposed in the literature.

**KEYWORDS:** Histogram, Threshold, Entropy, Filtering, Clustering, Logistic Regression.

---

## 1. Introduction

Alzheimer's disease (AD) is one of the chief brain abnormality, commonly found in the elderly people (people with age >60 years). The main cause of this disease is weakening the memory and the thinking ability and severe AD will cause the loss of memory. If the disease is detected in its premature phase, prescribed treatment and practice can be given to retain the memory or we can help the elderly people to take care of their common activity without any trouble. In the literature, a number of AD detection procedures are proposed and implemented by the researchers. This prohibits a person from carrying out day to day actions in a normal manner. It was estimated that around 5.3 million Americans suffer from this disorder in the year 2015. Hence, early diagnosis of this ailment is essential so that the affected person can be treated and the progression of the disorder can be ceased. Recently, the analysis of MRI data has been widely utilized for the diagnosis of AD. These images have various advantages like good resolution, high contrast, etc. The analysis of MRI images for AD diagnosis can be grouped into various categories based on grey matter voxels [17, 8, 37, 10, 27], morphometric systems [34], volume and regions of interest [18, 4, 11, 12, 9, 40], etc. Various machine learning algorithms have been widely used for the classification of AD [16, 15, 1, 6].

Hence, in this research we propose a novel framework for detection and classification of AD using MRI data.

The overall contributions of this paper are fourfold:

- a A new AD classification framework using MRI images is presented.
- b A novel image enhancement technique using ECLAHE algorithm is proposed.
- c A new image clustering technique using Enhanced Expectation Maximization (EEM) algorithm is presented.
- d A novel Adaptive Histogram (AH) thresholding algorithm is proposed.

The remaining paper is organized in the following way. Section 2 includes a detailed literature survey of the previous works in the literature. Section 3 describes the proposed methodology. The results and discussion are performed in Section 4. Conclusion of the paper is presented in Section 5.

---

## 2. Literature Survey

A system for AD detection using MRI images was proposed in [5]. In this paper, Convolutional Neural

Network was used for detection of AD. This system achieved a high accuracy of 99% using ADNI dataset and an accuracy of 98% using a combination of ADNI and non-ADNI dataset.

The authors of [21] proposed a system for AD diagnosis using deep learning technique. This paper detailed a review of different frameworks proposed in the literature based on deep learning techniques for the classification of AD. It was inferred that algorithms like Convolutional and Recurrent Neural Networks produced average accuracy of 96% for AD classification.

Detection of AD using CNN was presented in [36]. This framework used Grey Wolf Optimization technique to achieve a high recognition rate. Texture and histogram features were derived from the magnetic resonance imaging data. This framework achieved an average accuracy of about 96.23%

A review on various deep learning and feature extraction-based techniques for AD identification was presented in [25]. Here a new technique for fusion of data belonging to different modalities was also presented. CNN was used for the classification. The proposed system was also compared with a single modality framework.

Multi-class classification of AD using Grey Level Co-occurrence Matrix was proposed in [3]. In this work the data was classified into three classes. These included AD, normal and the mild cognitive impairment. This system achieved an overall accuracy of about 78.9% for the classification of the three classes.

Leaky Rectified Unit was used for the classification of AD in [39]. Here an eight layered-Convolutional Neural Network was employed. Three different pooling functions were used in this paper. These pooling functions included the stochastic pooling, the maximum pooling and the average pooling. This system achieved an accuracy of 97.65%.

Linear Discriminant Analysis and SVM algorithms were used for the classification of AD in [2]. Here dimensionality reduction was achieved using kernel principal component analysis technique. This system achieved an average classification accuracy of about 93.85% for ADNI database.

Prediction of AD using deformation of MRI data was proposed in [29]. This was based on the computation of morphological differences. This framework operated in three steps. The first step was the Diffeomorphic

Registration. The next step was the embedding step. The final step was the classification approach.

Various classification systems used for the diagnosis of AD was compared in [23]. Here a dataset generated from 70-year-old people was employed for classification. It was inferred that around 46% of the people suffered from AD.

Classification of patients with AD and Mild Cognitive Impairment was proposed in [31]. Here deep learning CNN was used for classification. Also Multi-layered feed forward perceptron (MLP) architecture was employed. This system achieved an overall accuracy of about 80%.

Various parameters of MRI images were combined for the classification of AD in [38]. In this work six major features were extracted. These included the area, thickness and the curvature of the cortical layer, density of grey matter etc. These features achieved a high AUC value of about 0.98.

The authors of [35] proposed a method for classifying mild and moderate state of AD. This system utilized an elastic net classifier for classification. Two types of classification were analyzed in this work. This included unimodal and multi-modal classification. The unimodal classification achieved AUC of 0.909, whereas, multi-modal achieved 0.952.

A technique for multitask feature learning was proposed in [20]. Here multi-task feature learning technique was used to learn the features. This paper introduced manifold-based Laplacian Regularize technique. This technique helped to preserve the intrinsic characteristic of the multi-modal data.

Kernel SVM and decision tree were utilized for the identification of AD in [42]. Here, initially MRI data was pre-processing using Atlas normalization. Then, the images were unsampled. The next step was feature extraction. This was performed using principal component analysis. Finally, classification was done using SVM.

Diagnosis of AD using sparse representation theory was presented in [19]. Nine different classification techniques were analyzed in this paper. This paper introduced penalized regression technique for binary classification.

Linear Embedding of MRI data for identification of people with Alzheimer's disorder was given by the authors of [28]. Here, local linear embedding (LLE) technique was used. ADNI database was used for sim-

ulation. It was observed that LLE was a very effective technique for classification of MRI data.

An automated multimodal classification method using deep learning for brain tumor type classification using BraTS datasets was presented in [24].

An efficient mixture classification technique which uses electro encephalography (EEG) signals for establishing a communication channel for the physically challenged people was given by [26].

Adaptive independent subspace analysis (AISA) method to discover meaningful electroencephalogram activity in the MRI scan data. The classification results were achieved using the k-nearest neighbor classifier with 10-fold cross-validation in [22]. Brain Computer Interface Systems to identify innovative, current, and great contribution works to the field of neuroscience was presented in [13].

### 3. Proposed Methodology

The proposed methodology comprises of steps like image preprocessing (filtering and enhancement), segmentation, feature extraction, dimensionality reduction and classification. This is depicted in Figure 1. The noisy MRI is initially acquired. This image is pre-processed using filtering and enhancement. Filtering is done to remove noise and enhancement is done to increase the contrast and details of the image. From the enhanced image, the region of interest (ROI) is segmented using image segmentation. Then, from the segmented regions, the features are extracted. The dimension of these features is reduced and finally the image is classified to two groups namely AD and normal.

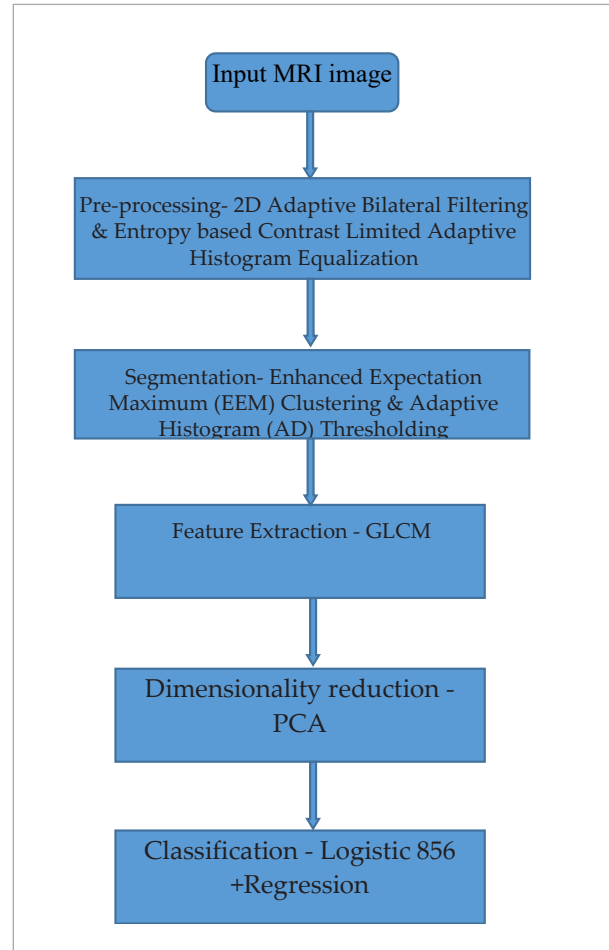
#### 3.1. Image Pre-processing

Pre-processing was performed using two steps namely, filtering and enhancement. Image filtering was performed using 2D Adaptive Bilateral Filter (2D-ABF) and enhancement was performed using a novel Entropy-based Contrast Limited Adaptive Histogram Equalization (ECLAHE) algorithm.

##### 3.1.1. Image Filtering Using 2D Adaptive Bilateral Filters

The input image  $X \in R^{U \times V}$  were first filtered using 2D Adaptive Bilateral Filters. The output obtained is  $Y \in$

**Figure 1**  
Classification of MRI Images



$R^{U \times V}$ . The bilateral filtering operation is defined and shown in Equation (1).

$$y[u, v] = \sum_k \sum_l R^{-1}(k, l) h_d(u, v; k, l) h_r(x[u, v], x[k, l]) x[k, l] \tag{1}$$

where  $x[u, v]$  represents the input image and  $y[u, v]$  represents the filtered output. Also,  $h_d$  and  $h_r$  represents domain and range filters, respectively. They are represented as

$$h_d(u, v; u_0, v_0) = e^{-\left(\frac{(u-u_0)^2 + (v-v_0)^2}{2\sigma_d^2}\right)} \tag{2}$$

$$h_r(x[u, v], x[u_0, v_0]) = e^{-\left(\frac{(x[u, v] - x[u_0, v_0])^2}{2\sigma_r^2}\right)} \tag{3}$$

Here  $[u_0, v_0]$  represents the center pixel. Also,  $\sigma_d$  and  $\sigma_r$  represents the standard deviation of the domain and range filter respectively.

The above two equations were modified by [43] by including an offset component. Thus, the modified 2D Adaptive Bilateral filters are defined as

$$h_d(u, v; u_0, v_0) = e^{-\left(\frac{(u-u_0)^2+(v-v_0)^2}{2\sigma_d^2}\right)} \quad (4)$$

$$h_r(x[u, v], x[u_0, v_0]) = e^{-\left(\frac{(x[u, v]-x[u_0, v_0]-\zeta[u_0, v_0])^2}{2\sigma_r^2}\right)} \quad (5)$$

The sharpness of the image is controlled by  $\zeta$ . The image gets blurred when the value of  $\zeta$  is moved closer to the mean. However, by moving it away from the mean, the filtered image gets sharper.

### 3.1.2. Image Enhancement Using Entropy-based CLAHE (ECLAHE) Algorithm

The filtered images were then enhanced using a novel Entropy-based CLAHE (ECLAHE) algorithm. This system is given in Algorithm 1. The main objective of the proposed algorithm is to preserve the regions containing edge information in the images. Since the adaptive histogram equalization technique equalizes the histogram of an image in a uniform manner, the edge information gets degraded. To avoid this, in the proposed algorithm we have initially identified the regions containing edges. The histogram equalization is not applied for the edge regions. That is, the entire image is first divided into four groups namely, the High Entropy Blocks (HEB), Corner Blocks (CB), Border Blocks (BB) and the Low Entropy Blocks (LEB). To preserve the edge and corner details, the High Entropy, Corner and Border Blocks are retained. This is based on the fact that; the entropy or information content will be high in the edge regions compared to the smooth regions. The equalization of the histogram is applied only for the Low Entropy Blocks.

**Algorithm 1:** Proposed Entropy-based CLAHE (ECLAHE) technique.

Input:

Filtered image  $Y \in R^{U \times V}$ .

Output:

Enhanced image  $I^E \in R^{U \times V}$ .

Steps:

- 1 Divide the entire image  $Y \in R^{U \times V}$  into non-overlapping blocks of size  $n \times n$ .
- 2 Compute entropy of each non-overlapping block and normalize the values using  $l_2$ -norm.
- 3 From the entropy values identify the blocks that comprises of entropy values greater than threshold  $\lambda$ . These blocks are identified as High Entropy Blocks (HEB).
- 4 Identify the four corner blocks as Corner Blocks (CB).
- 5 The border blocks other than the four corner blocks are identified as Border Blocks (BB).
- 6 The remaining blocks are identified as the Low Entropy Blocks (LEB).
- 7 Compute the histogram of each region.
- 8 Obtain uniform density function for the ISB regions by computing the CDF [41] of the histogram using,

$$C_{i,j}(n) = \frac{(N-1)}{M} \sum_{k=0}^n h_{i,j}(k); n = 1, 2, \dots, N-1.$$

- 9 Map every pixel in the LEB by linear combination of results obtained from four nearest regions to obtain the Enhanced image  $I^E \in R^{U \times V}$ .

## 3.2. Segmentation

Segmentation is performed using clustering and thresholding techniques. Clustering is performed using Enhanced Expectation Maximum algorithm and thresholding is done using Adaptive Histogram technique. They are described in detail in the following sections.

### 3.2.1. Enhanced Expectation Maximum (EEM) Clustering

We have proposed a new clustering algorithm to obtain clusters from the enhanced images. This is based on Expectation Maximum algorithm [14]. In this algorithm, there are two main steps, namely, the Expectation step and the Maximization step. They are described below.

Expectation step:

The probability that a pixel at  $I^E(u, v)$  belongs to a particular Gaussian  $G_i$  with mean  $\mu_i$  and standard deviation  $\sigma_i$  is given by

$$P_{uv}^i = \frac{\exp\left(-\frac{(I^E(u,v)-\mu_i)^2}{2\sigma_i^2}\right)}{\sum_{j=1}^V \exp\left(-\frac{(I^E(u,v)-\mu_j)^2}{2\sigma_j^2}\right)} \quad (6)$$

**Maximization step:**

In this step, the values of mean  $\mu_i$  and standard deviation  $\sigma_i$  of the Gaussian  $G_i$  are estimated again using

$$\mu_i = \frac{1}{Z} \sum_{u,v} P_{uv}^i I^E(u, v) \quad (7)$$

$$\sigma_i = \sqrt{\frac{\sum_{u,v} P_{uv}^i (I^E(u,v)-\mu_i)^2}{Z}} \quad (8)$$

The above two expectation and maximization steps are iterated until convergence state is achieved. The quality of clustering result obtained mainly depends on the initial values of the EM algorithm. In a conventional EM algorithm, these initial values are obtained using k-means algorithm. To further improve the accuracy and reliability of clustering result, in this work, we propose novel Enhanced Expectation Maximization algorithm. In this algorithm, instead of using k-means, the initial values are computed using Fuzzy C Means Clustering [7]. That is, the initial values are computed using

$$J = \sum_{i=0}^{255} \sum_{q=1}^C f_{iq} d(i, \theta_q) \quad (9)$$

where  $f_{iq}$  refers to the fuzzy membership between pixel  $x_i$  and histogram of cluster with center  $\theta_q$  and  $d(i, \theta_q)$  refers to the distance between pixel  $x_i$  and histogram of cluster with center  $\theta_q$ . The output of clustering step is represented as  $I^C \in R^{U \times V}$ .

**3.2.2. Adaptive Histogram (AD) Thresholding**

Otsu threshold [32] is a widely used technique for image segmentation. It identifies a global threshold for segmenting an image into two categories namely, the foreground and the background. Every pixel value in an image is compared with the threshold. If the value of the pixel is greater than the threshold, then it is classified as foreground, else it is classified as a background pixel. However, this thresholding technique does not produce accurate results when the illumination of the background is uneven. Hence, in this work we have employed adaptive thresholding technique.

In this technique, the threshold used for segmentation is not global. The value of threshold varies as a function of the location in the image. In our proposed method, the adaptive threshold is computed based on histogram. The image is initially divided into several non-overlapping blocks. Then for each block the histogram is computed. Then the highest two peaks in the histogram is identified. These peaks represent the pixels that are dominant in the block. Then the adaptive threshold for that particular block is identified as the average of the two peak values. The proposed novel AD thresholding algorithm is given in Algorithm 2.

**Algorithm 2:** Proposed Adaptive Histogram (AH) Thresholding.

**Input:**

Clustered image  $I^C \in R^{U \times V}$ .

**Output:**

Segmented image  $I^S \in R^{U \times V}$ .

**Steps:**

- 1 Divide the entire image  $I^C \in R^{U \times V}$  into non-overlapping blocks of size  $n \times n$ .
- 2 Compute the histogram of each block  $B_i$ .
- 3 Identify the highest two peaks  $P_1$  and  $P_2$  in the histogram of each block.
- 4 The threshold  $T_i$  for block  $B_i$  is computed as  $T_i = \frac{P_1 + P_2}{2}$
- 5 Segment the pixels  $I_i^C(u, v)$  in block  $B_i$  using

$$I_i^S(u, v) = \begin{cases} 1; & I_i^C(u, v) \geq T_i \\ 0; & I_i^C(u, v) < T_i \end{cases}$$

**3.3. Feature Extraction**

In this work, we have extracted Gray-Level Co-Occurrence Matrix features [44]. This feature exploits the special relationship between two pixels that are spaced by a particular distance in an image. The GLCM feature has a rapidly changing value in fine texture regions and a slowly changing value in the coarse texture regions. It is computed as

$$G(m, n) = \frac{\#\{(m_1, n_1), (m_2, n_2)\} \in S \mid f(m_1, n_1) = g_1 \& f(m_2, n_2) = g_2\}}{\#S} \quad (10)$$

Using this technique several statistical features like contrast, energy, homogeneity, correlation was extracted.

**Angular second moment:**

Angular second moment represents the uniformity of the distribution of the image. It is computed as

$$A_{sm} = \sum_m^M \sum_n^N G(m, n)^2 \quad (11)$$

**Correlation:**

Correlation value indicates the similarity of the texture of the image in the two perpendicular directions namely, the horizontal and the vertical directions. It is computed using

$$C_{or} = \frac{\sum_m^M \sum_n^N (m-\bar{x})(n-\bar{y})G(m, n)}{\sigma_x \sigma_y} \quad (12)$$

**Contrast:**

Contrast value indicates the variation of depth and smooth regions of the image and is computed as

$$C_{on} = \sum_m^M \sum_n^N (m - n)^2 G(m, n) \quad (13)$$

**Entropy:**

Entropy is the measure of information content and is computed using

$$E_{nt} = - \sum_m^M \sum_n^N G(m, n) I_g G(m, n) \quad (14)$$

**3.4. Dimensionality Reduction Using PCA**

The principal components of the extracted features are computed to improve the classification accuracy. Here, first covariance matrix  $CM$  is computed using the extracted features of dimension  $N$ . Then, Eigen values and corresponding Eigen vectors are computed for the covariance matrix  $CM$ . The eigen vectors that are corresponding to the  $K$  largest eigen values are identified as the principal components. Finally, dimensionality reduction is done by projecting the features to a lower dimensional space using the generated principal components.

**3.5. Alzheimer's Disease Classification on MRI Brain Image**

From these obtained low-dimensional features, classification models are created during the training phase. Using the classification model, classification is done in the testing phase. In our work, we have em-

ployed the Logistic Regression (LR) [33] for classification of tumor images. In logistic regression, a feature vector  $z = (z_1, z_2, \dots, z_q)$  is classified to a class  $y \in \{0, 1\}$  using

$$P(y = 0/z) = \frac{1}{1 + e^{z\beta + \beta_0}} \quad (15)$$

$$P(y = 1/z) = \frac{e^{z\beta + \beta_0}}{1 + e^{z\beta + \beta_0}} \quad (16)$$

where  $\beta = (\beta_1, \beta_2, \dots, \beta_q)$  represents the weight vector and  $\beta_0$  represents the intercept value. A test data sample is classified to a particular class by first evaluating the two probabilities namely the,  $P(y = 0/z)$  and  $P(y = 1/z)$ , and then assigning to the class that has a higher probability.

**4. Results and Discussion****4.1. Parameter Settings**

The proposed system was simulated using MATLAB software running on windows intel i3 core processor with 6GB RAM. Four different MRI images were considered for analysis on our work. The value of threshold in Algorithm 1 was selected as 0.75. The value of used for creating blocks in both Algorithm 1 and Algorithm 2 was set as 16.

**4.2. Simulation Results**

The total number of images considered in this research work is shown in Table 1.

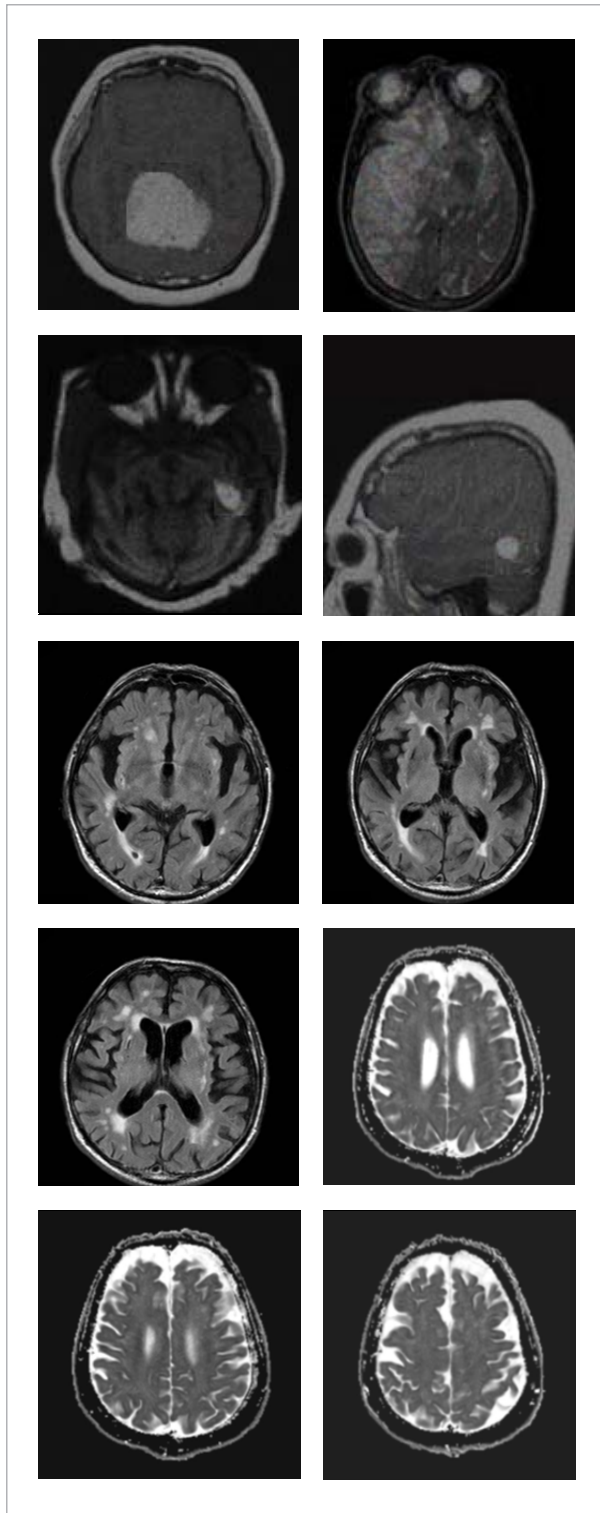
**Table 1**

Total Images

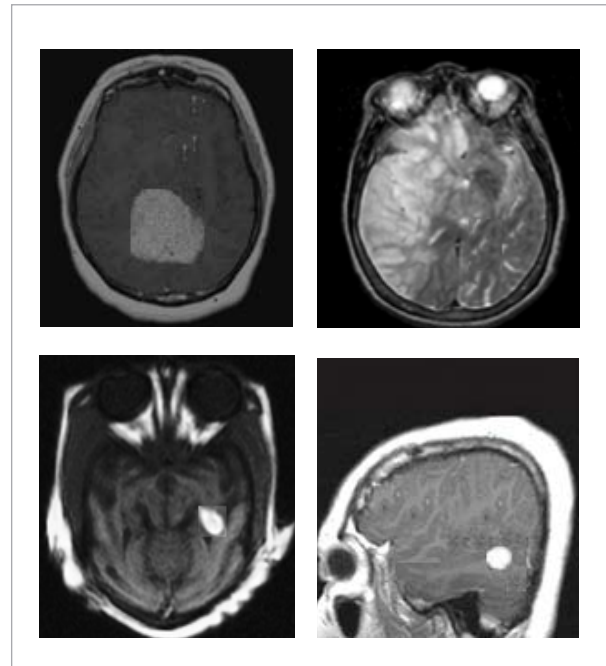
Class	Total images	Classifier	
		Training	Validation
Normal	300	200	100
AD	300	200	100

Figure 2 shows the input noisy MRI images. This image has noise and hence cannot be processed directly. Figure 3 shows the 2D Adaptive Bilateral filtered MRI images. From Figure 3 we infer that the filtered images have less noise compared to the original images.

**Figure 2**  
Input Noisy MRI Images



**Figure 3**  
2D Adaptive Bilateral filtered MRI Images



Hence, the tumor regions are more prominently perceived compared to the original images.

Figure 3 shows the 2D Adaptive Bilateral filtered MRI images. From Figure 3 we infer that the filtered images have less noise compared to the original images. Hence, the tumor regions are more prominently perceived compared to the original images.

Figure 4 shows ECLAHE MRI enhanced images. From Figure 4, it is obvious that the enhanced images have better clarity and contrast compared to the original images. This aids in achieving better segmentation results that in turn help in achieved accurate classification results.

Figure 5 shows normal and abnormal image segmentation results using EEM clustering and AH thresholding. The segmentation results clearly show the regions containing the tumor cells. From these segmented regions, the features are extracted. These features are then classified to AD and normal classes using classification algorithms. From Figure 5, we see that the second image does not contain any tumor region. However, all the other three images contain tumor regions.



Figure 4

ECLAHE MRI enhanced Images

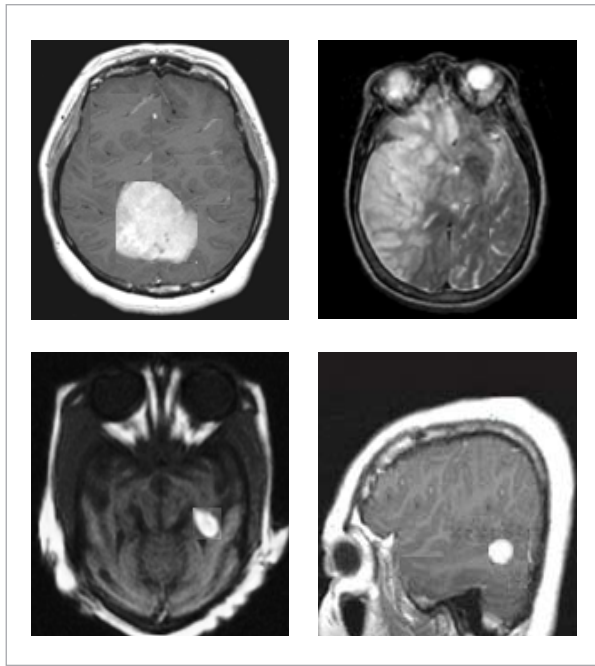
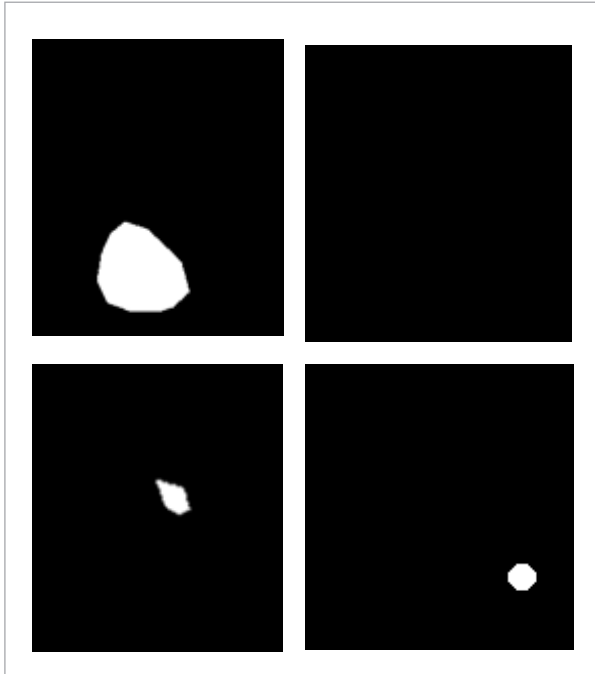


Figure 5

Image segmentation using EEM clustering and AH thresholding



### 4.3. Quantitative Analysis

#### 4.3.1. Evaluation of Proposed Pre-processing (2D-ABF-ECLAHE) Algorithms

Mean Square Error (MSE):

MSE gives the average difference between the original image  $O$  and the filtered-enhanced image  $E$  after applying the filtering and enhancement algorithm. It is given by

$$(1/N^2) \sum_{i=1}^N \sum_{j=1}^N [O(i,j) - E(i,j)]^2 \quad (17)$$

Peak Signal to Noise Ratio (PSNR):

PSNR gives the ratio of signal value to the error value. Higher the PSNR higher the quality. It is calculated as

$$PSNR = 10 \log_{10} \frac{255^2}{(1/N^2) \sum_{i=1}^N \sum_{j=1}^N [O(i,j) - E(i,j)]^2} \quad (18)$$

Table 2 shows the performance evaluation using mean square error. From Table 2 we see that, the average value of MSE for a combination of 2D Median Filter with CLAHE algorithm is 6.92. Similarly, the average value of MSE for a combination of 2D Adaptive Median Filter with CLAHE algorithm is 3.29. However, our proposed 2D-ABF Filter with ECLAHE algorithm produces a very low MSE of 0.80. Thus, the proposed pre-processing technique achieves best performance in terms of MSE.

Table 2

Performance Evaluation using Mean Square Error

Image Number	2D Median Filter + CLAHE	2D Adaptive Median Filter + CLAHE	Proposed 2D-ABF Filter + ECLAHE
1	6.13	2.98	0.73
2	6.97	3.83	0.81
3	7.32	2.13	0.87
4	7.28	3.92	0.82

Table 3 shows the performance evaluation using mean Peak Signal to Noise Ratio. From Table 2 we see that, the average value of PSNR for a combination of 2D Median Filter with CLAHE algorithm is 22.46. Similarly, the average value of PSNR for a combination of 2D Adaptive Median Filter with CLAHE algo-

**Table 3**

Performance Evaluation using PSNR

Image Number	2D Median Filter + CLAHE	2D Adaptive Median Filter + CLAHE	Proposed 2D-ABF Filter + ECLAHE
1	23.12	28.12	33.02
2	21.43	24.71	36.52
3	24.79	25.41	35.21
4	20.52	26.80	34.69

rithm is 26.26. However, our proposed 2D-ABF Filter with ECLAHE algorithm produces a very high PSNR of 34.86. Thus, our proposed pre-processing technique achieves best performance in terms of PSNR.

#### 4.3.2. Evaluation of Segmentation Algorithms

Jaccard coefficient is commonly used for evaluating the performance of segmentation algorithms. It is given by

$$J(O_a) = \frac{B \cap G}{B \cup G} \quad (19)$$

where  $O_a$  is the overlap area,  $B$  is the binary image and  $G$  is the ground truth image.

The Dice coefficient is computed as

$$D(B, G) = \frac{2|B \cap G|}{|B| + |G|} \quad (19)$$

Its value ranges between 0 to 1. A value of 0 refers to a condition with no overlap and 1 refers to a condition with complete overlap.

Table 3 shows the performance evaluation using Jaccard Coefficient. From Table 4 we infer that, the average value of Jaccard Coefficient for K means clustering with Otsu thresholding was 0.5265. Similarly, the average value of Jaccard Coefficient for Fuzzy C Means Clustering with Otsu thresholding was 0.6261. But the proposed EEM Clustering with proposed AD thresholding achieved a maximum Jaccard Coefficient of 0.8004. Thus, the proposed framework achieves best performance in terms of Jaccard Coefficient.

Table 5 shows the performance evaluation using Dice Coefficient. From Table 4 we infer that, the average value of Dice Coefficient for K means clustering with Otsu thresholding was 0.5549. Similarly, the average

**Table 4**

Performance Evaluation using Jaccard Coefficient

Image set	K means clustering + Otsu Thresholding	Fuzzy C Means Clustering + Otsu Thresholding	Proposed EEM Clustering + AD Thresholding
1	0.4446	0.6534	0.8522
2	0.5732	0.6434	0.7523
3	0.5152	0.5645	0.8534
4	0.5733	0.6431	0.7439

**Table 5**

Performance Evaluation using Dice Coefficient

Image set	K means clustering + Otsu Thresholding	Fuzzy C Means Clustering + Otsu Thresholding	Proposed EEM Clustering + AD Thresholding
1	0.5192	0.6248	0.7234
2	0.5269	0.6231	0.9274
3	0.5787	0.6631	0.7252
4	0.5951	0.6158	0.8352

value of Dice Coefficient for Fuzzy C Means Clustering with Otsu thresholding was 0.6317. But the proposed EEM Clustering with proposed AD thresholding achieved a maximum Dice Coefficient of 0.8028. Thus, our proposed framework achieves best performance in terms of Dice Coefficient.

#### 4.3.3. Evaluation of Classification Algorithms

To evaluate the classification performance, metrics like overall accuracy, recall, precision, specificity and F-score were employed. For evaluation we employed the Open Access Series of Imaging Studies (OASIS) dataset [30] that consists of 416 sample with ages varying from 18 to 96. We performed ten-fold cross validation.

To evaluate the classification performance, initially true positive (TP), true negative (TN), false positive (FP) and false negative (FN) were computed.

TP: It gives the count of AD cases present and detected.

TN: It gives the count of AD cases not present and not detected.

FP: It gives the count of AD cases not present but detected as AD.

FN: It gives the count of AD cases present but not detected as AD.

From the above computed parameters, classification metrics like overall accuracy, recall, precision, specificity and F-score were calculated.

#### Overall accuracy:

Overall accuracy indicates the overall classification performance of the classifier to identify AD.

$$Accuracy = \frac{TP+TN}{TP+TN+FP+FN} \quad (21)$$

#### Recall:

The recall refers to the sensitivity of classification for the detection of AD and is computed as

$$Recall = \frac{TP}{TP+FN} \quad (22)$$

#### Precision:

The precision is the ratio of number of true positives to the sum of true positives and false positives.

$$Precision = \frac{TP}{TP+FP} \quad (23)$$

#### Specificity:

The specificity is the ratio of number of true negatives to the sum of true negatives and false positives

$$Specificity = \frac{TN}{TN+FP} \quad (24)$$

#### F-score:

The F-score is computed as

$$F - score = 2 \times \frac{Precision \times Recall}{Precision + Recall} \quad (25)$$

The classification is also performed using traditional algorithms like k-nearest neighbour (k-NN), Naïve Bayes, Random Forest, support vector machine (SVM) for comparison. Table 5 shows the results obtained in terms of overall accuracy. From Table 6, we see that Logistic Regression algorithm produces the best results compared to all other traditional classification algorithms.

**Figure 6**  
Comparison of specificity

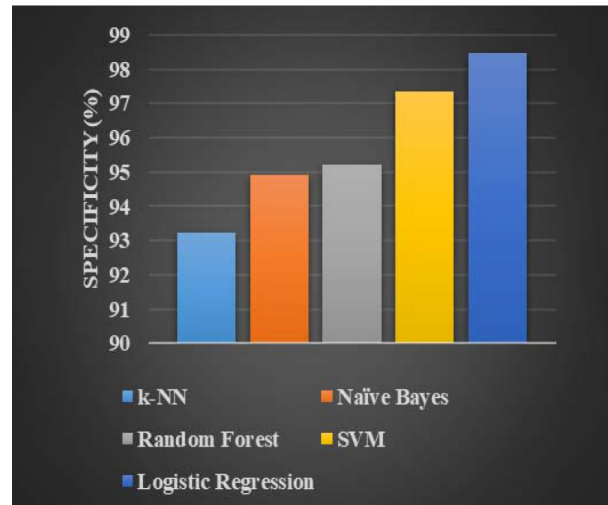


Figure 6 represents the comparison of specificity for the four image sets. From Figure 6 we see that the value of specificity obtained by k-NN, Naïve Bayes, Random Forest, SVM and Logistic Regression are 93.23, 94.92, 95.23, 97.34 and 98.49 respectively. Thus, it is clearly seen that Logistic Regression outperforms other algorithms.

**Table 6**

Comparison of overall accuracy

Classifier	TP	FN	TN	FP	Precision	Sensitivity	Specificity	FScore	Accuracy
k-NN	92	8	88	12	88.4615	92	88	90.1961	90.39
Naïve Bayes	91	9	92	8	91.9192	91	92	91.4573	92.19
Random Forest	93	7	91	9	91.1765	93	91	92.0792	92.98
SVM	94	6	93	7	93.0693	94	93	93.5323	93.82
Proposed Logistic Regression	97	5	98	4	96.95	95.63	98.49	96.21	<b>96.92</b>

**Figure 7**

Comparison of precision

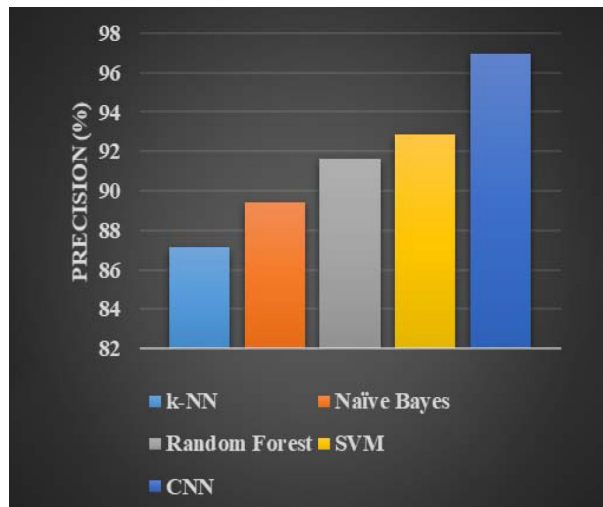


Figure 7 represents the comparison of precision for the four image sets. From Figure 7 we see that the average value of precision obtained by k-NN, Naïve Bayes, Random Forest, SVM and Logistic Regression are 87.13, 89.42, 91.6, 92.89 and 96.95 respectively. Thus, it is clearly seen that Logistic Regression is the best compared to other algorithms.

Figure 8 represents the comparison of recall for the four image sets. From Figure 8 we see that the average value of recall obtained by k-NN, Naïve Bayes, Random Forest, SVM and Logistic Regression are 90.23, 91.92, 92.23, 91.82 and 95.63 respectively. Thus, it is clearly seen that Logistic Regression performs better than other traditional classification algorithms.

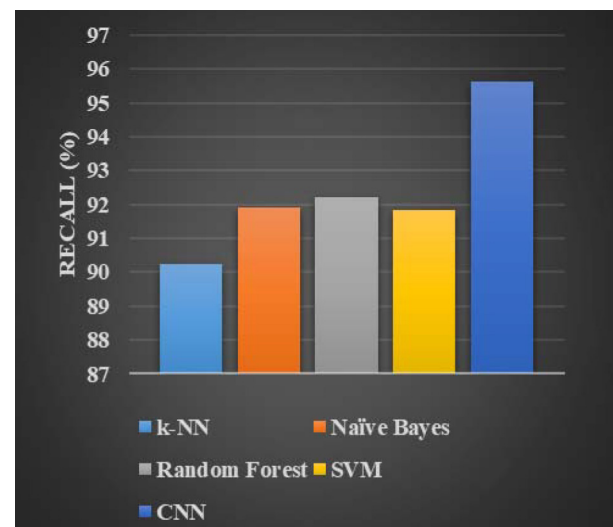
Figure 9 represents the comparison of F-score for the four image sets. From Figure 9 we see that the average value of F-score obtained by k-NN, Naïve Bayes, Random Forest, SVM and Logistic Regression are 90.23, 91.42, 92.63, 93.12 and 96.21 respectively. Thus, the F-score of Logistic Regression is better than other algorithms.

## 5. Conclusion

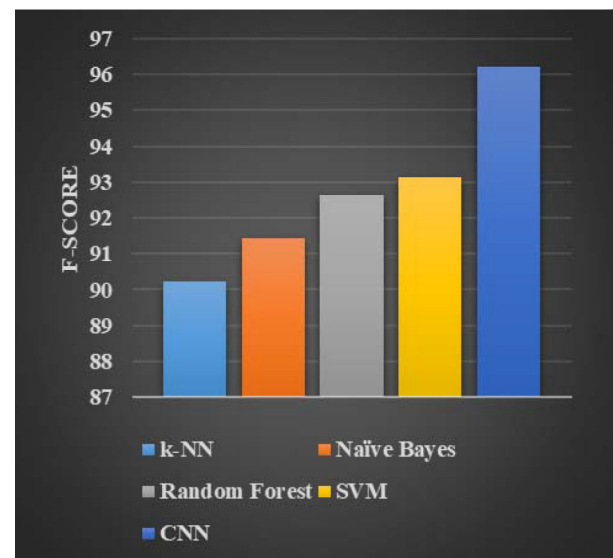
In this research we proposed a novel approach for novel framework for the detection and classification of AD using image processing techniques. Here, we employed 2D Adaptive Bilateral Filter (2D-ABF)

**Figure 8**

Comparison of recall

**Figure 9**

Comparison of F-Score



for noise removal. The denoised image was then enhanced using Entropy-based Contrast Limited Adaptive Histogram Equalization (ECLAHE) algorithm. Clustering was performed using Enhanced

Expectation Maximization (EEM) and thresholding was performed using Adaptive Histogram (AH) thresholding algorithm. From the ROI, features were extracted using GLCM. The dimension of these features was then reduced using Principle Component Analysis (PCA). Finally, the obtained features were classified using Logistic Regression. The performance of the proposed pre-processing framework was evaluated in terms of MSE and PSNR. It was observed that the proposed 2D-ABF Filter with ECLAHE algorithm produces very low MSE of 0.80 and high PSNR of about 34.86. Also, the credibility of the segmentation methodology was proved using Jaccard and Dice coefficients. It was observed that

the proposed EEM Clustering with proposed AD thresholding achieved an average Jaccard and Dice coefficient values of 0.8004 and 0.8028 respectively. Finally, the Logistic Regression classification algorithm was compared with traditional machine learning algorithms like k-NN, Naive Bayes, random forest and SVM in terms of metrics like accuracy, specificity, precision, recall and F-score. It was observed that Logistic regression produced excellent results in terms of all the classification metrics. In particular, the logistic regression achieved an overall accuracy of about 96.92%. Also, it attained 98.49%, 96.95%, 95.63% and 96.21% in terms of specificity, precision, recall and F-score respectively.

## References

1. Aguilar, C., Westman, E., Muehlboeck, J.-S., Mecocci, P., Vellas, B., Tsolaki, M., Kloszewska, I., Soininen, H., Lovestone, S., Spenger, C., Simmons, A., Wahlund, L.-O. Different Multivariate Techniques for Automated Classification of MRI Data in Alzheimer's Disease and Mild Cognitive Impairment. *Psychiatry Res. - Neuroimaging*, 2013, 212(2), 89-98. <https://doi.org/10.1016/j.psychresns.2012.11.005>
2. Alam, S., Kwon, G. R. Alzheimer Disease Classification Using KPCA, LDA, and Multi-kernel Learning SVM. *International Journal of Imaging Systems and Technology*, 2017, 27(2), 133-143. <https://doi.org/10.1002/ima.22217>
3. Altaf, T., Anwar, S. M., Gul, N., Majeed, M. N., Majid, M. Multi-class Alzheimer's Disease Classification Using Image and Clinical Features. *Biomedical Signal Processing and Control*, 2018, 43, 64-74. <https://doi.org/10.1016/j.bspc.2018.02.019>
4. Barnes, J., Scahill, R. I., Boyes, R. G., Frost, C., Lewis, E. B., Rossor, C. L., Rossor, M. N., Fox, N. C. Differentiating AD from Aging Using Semiautomated Measurement of Hippocampal Atrophy Rates. *Neuroimage*, 2004, 23(2), 574-581. <https://doi.org/10.1016/j.neuroimage.2004.06.028>
5. Basaia, S., Agost, F., Wagner, L., Canu, E., Magnan, G., Santangelo, R., Filippi, M. Automated Classification of Alzheimer's Disease and Mild Cognitive Impairment Using a Single MRI and Deep Neural Networks. *Neuroimage: Clinical*, 2019, 21, 101645. <https://doi.org/10.1016/j.nicl.2018.101645>
6. Beheshti, I., Demirel, H. Feature-ranking-based Alzheimer's disease Classification from Structural MRI. *Magnetic Resonance Imaging*, 2016, 34(3), 252-263. <https://doi.org/10.1016/j.mri.2015.11.009>
7. Bezdek, J. C., Ehrlich, R., Full, W. FCM: The Fuzzy c-means Clustering Algorithm. *Computers and Geosciences*, 1984, 10(2-3), 191-203. [https://doi.org/10.1016/0098-3004\(84\)90020-7](https://doi.org/10.1016/0098-3004(84)90020-7)
8. Bozzali, M., Filippi, M., Magnani, G., Cercignani, M., Franceschi, M., Schiatti, E., Castiglioni, S., Mossini, R., Falautano, M., Scotti, G., Comi, G., Falini, A. The Contribution of Voxel-based Morphometry in Staging Patients with Mild Cognitive Impairment. *Neurology*, 2005, 67(3), 453-460. <https://doi.org/10.1212/01.wnl.0000228243.56665.c2>
9. Busatto, G. F., Garrido, G. E. J., Almeida, O. P., Castro, C. C., Camargo, C. H. P., Cid, C. G., Buchpiguel, C. A., Furuie, S., Bottino, C. M. A Voxel-based Morphometry Study of Temporal Lobe Gray Matter Reductions in Alzheimer's Disease. *Neurobiology of Aging*, 2003, 24(2), 221-231. [https://doi.org/10.1016/S0197-4580\(02\)00084-2](https://doi.org/10.1016/S0197-4580(02)00084-2)
10. Chételat, G., Landeau, B., Eustache, F., Mézenge, F., Viader, F., de la Sayette, V., Desgranges, B., Baron, J.-C. Using Voxel-based Morphometry to Map the Structural Changes Associated with Rapid Conversion in MCI: A Longitudinal MRI Study. *Neuroimage*, 2005, 27(4), 934-946. <https://doi.org/10.1016/j.neuroimage.2005.05.015>
11. Colliot, O., Chételat, G., Chupin, M., Desgranges, B., Magnin, B., Benali, H., Dubois, B., Garnero, L., Eustache, F., Lehericy, S. Discrimination Between Alzheimer

- Disease, Mild Cognitive Impairment, and Normal Aging by Using Automated Segmentation of the Hippocampus. *Radiology*, 2008, 248(1), 194-201. <https://doi.org/10.1148/radiol.2481070876>
12. Cuingnet, R., Gerardin, E., Tessieras, J., Auzias, G., Lehericy, S., Habert, M.-O., Chupin, M., Benali, H., Colliot, O. Automatic Classification of Patients with Alzheimer's Disease from Structural MRI: A Comparison of Ten Methods Using the ADNI Database. *Neuroimage*, 2011, 56(2), 766-781. <https://doi.org/10.1016/j.neuroimage.2010.06.013>
  13. de Albuquerque, V. H. C., Damaševičius, R., Garcia, N. M., Pinheiro, P. R., Rebouças Filho, P. P. Brain Computer Interface Systems for Neurorobotics: Methods and Applications. *BioMed Research International*, 2017. <https://doi.org/10.1155/2017/2505493>
  14. Dempster, A. P., Laird, N. M., Rubin, D. B. Maximum Likelihood from Incomplete Data Via the EM Algorithm. *Journal of the Royal Statistical Society: Series B (Methodological)*, 1977, 39(1), 1-22. <https://doi.org/10.1111/j.2517-6161.1977.tb01600.x>
  15. Gerardin, E., Chételat, G., Chupin, M., Cuingnet, R., Desgranges, B., Kim, H.-S., Niethammer, M., Dubois, B., Lehericy, S., Garnero, L., Eustache, F., Colliot, O. Multidimensional Classification of Hippocampal Shape Features Discriminates Alzheimer's Disease and Mild Cognitive Impairment from Normal Aging. *Neuroimage*, 2009, 47(4), 1476-1486. <https://doi.org/10.1016/j.neuroimage.2009.05.036>
  16. Gutman, B., Wang, Y., Morra, J., Toga, A. W., Thompson P. M. Disease Classification with Hippocampal Shape Invariants. *Hippocampus*, 2009, 19(6), 572-578. <https://doi.org/10.1002/hipo.20627>
  17. Hirata, Y., Matsuda, H., Nemoto K, Ohnishi, T., Hirao, K., Yamashita, F., Asada, T., Iwabuchi, S., Samejima, H. Voxel-based Morphometry to Discriminate Early Alzheimer's Disease from Controls. *Neuroscience Letters*, 2005, 382(3), 269-274. <https://doi.org/10.1016/j.neulet.2005.03.038>
  18. Jack, C. R. Prediction of AD with MRI-based Hippocampal Volume in Mild Cognitive Impairment. *Neurology*, 1999, 52(7), 1397-1403. <https://doi.org/10.1212/WNL.52.7.1397>
  19. Janousova, E., Vounou, M., Wolz, R., Gray, K. R., Rueckert, R., Montana, G. Biomarker Discovery for Sparse Classification of Brain Images in Alzheimer's Disease. *Annals of the BMVA*, 2012, 1-11.
  20. Jie, B., Zhang, D., Cheng, B., Shen, D. Manifold Regularized Multitask Feature Learning for Multimodality Disease Classification. *Human Brain Mapping*, 2015, 36(2), 489-507. <https://doi.org/10.1002/hbm.22642>
  21. Jo, T., Nho, K., Saykin, A. J. Deep Learning in Alzheimer's Disease: Diagnostic Classification and Prognostic Prediction Using Neuroimaging Data. *Frontiers in Aging Neuroscience*, 2019, 11. <https://doi.org/10.3389/fnagi.2019.00220>
  22. Ke, Q., Zhang, J., Wei, W., Damaševičius, R., Woźniak, M. Adaptive Independent Subspace Analysis of Brain Magnetic Resonance Imaging Data. *IEEE Access*, 2019, 7, 12252-12261. <https://doi.org/10.1109/ACCESS.2019.2893496>
  23. Kern, S., Zetterberg, H., Kern, J., Zettergren, A., Waern, M., Höglund, K., Andreasson, U., Wetterberg, H., Börjesson-Hanson, A., Blennow, K., Skoog, I. Prevalence of Preclinical Alzheimer Disease: Comparison of Current Classification Systems. *Neurology*, 2018, 90(19), E1682-E1691. <https://doi.org/10.1212/WNL.0000000000005476>
  24. Khan, M. A., Ashraf, I., Alhaisoni, M., Damaševičius, R., Scherer, R., Rehman, A., Bukhari, S. A. C. Multimodal Brain Tumor Classification Using Deep Learning and Robust Feature Selection: A Machine Learning Application for Radiologists. *Diagnostics*, 2020, 10 (8), 565. <https://doi.org/10.3390/diagnostics10080565>
  25. Khvostikov, A., Aderghal, K., Benois-Pineau, J., Krylov, A., Catheline, G. 3D CNN-based Classification Using sMRI and MD-DTI Images for Alzheimer Disease Studies, 2018.
  26. Krishna, N. M., Sekaran, K., Vamsi, V. N., Pradeep Ghanatasala, G. S., Chandana, P., Kadry, S., Blažauskas, T., Damaševičius, R. An Efficient Mixture Model Approach in Brain-Machine Interface Systems for Extracting the Psychological Status of Mentally Impaired Persons Using EEG Signals. *IEEE Access*, 2019, 7, 77905-77914. <https://doi.org/10.1109/ACCESS.2019.2922047>
  27. Lao, Z., Shen, D., Xue, Z., Karacali, B., Resnick, S. M., Davatzikos, C. Morphological Classification of Brains Via High-dimensional Shape Transformations and Machine Learning Methods. *Neuroimage*, 2004, 21(1), 46-57. <https://doi.org/10.1016/j.neuroimage.2003.09.027>
  28. Liu, X., Tosun, D., Weiner, M. W., Schuff, N. Locally Linear Embedding (LLE) for MRI Based Alzheimer's Disease Classification. *Neuroimage*, 2013, 83, 148-157. <https://doi.org/10.1016/j.neuroimage.2013.06.033>
  29. Long, X., Chen, L., Jiang, C., Zhang, L. Prediction and Classification of Alzheimer Disease Based on Quantification of MRI Deformation. *PLoS One*, 2017, 12(3), 1-19. <https://doi.org/10.1371/journal.pone.0173372>

30. Marcus, D. S., Wang, T. H., Parker, J., Csernansky, J. G., Morris, J. C., Buckner, L. R. Open Access Series of Imaging Studies (OASIS): Cross-sectional MRI Data in Young, Middle Aged, Nondemented, and Demented Older Adults. *Journal of Cognitive Neuroscience*, 2007, 19(9), 1498-1507. <https://doi.org/10.1162/jocn.2007.19.9.1498>
31. Morabito, F. C., Campolo, M., Ieracitano, C., Ebadi, J. M., Bonanno, L., Bramanti, A., Desalvo, S., Mammonia, N., Bramanti, P. Deep Convolutional Neural Networks for Classification of Mild Cognitive Impaired and Alzheimer's Disease Patients from Scalp EEG Recordings. In 2016 IEEE 2nd International Forum on Research and Technologies for Society and Industry Leveraging a Better Tomorrow (RTSI), 2016, 1-6. <https://doi.org/10.1109/RTSI.2016.7740576>
32. Otsu, N. Threshold Selection Method from Gray-Level Histograms. *IEEE Transactions on Systems, Man, and Cybernetics*, 1979, SMC-9(1), 62-66. <https://doi.org/10.1109/TSMC.1979.4310076>
33. Rao, A., Lee, Y., Gass, A., Monsch, A. Classification of Alzheimer's Disease from Structural MRI Using Sparse Logistic Regression with Optional Spatial Regularization. In 2011 Annual International Conference of the IEEE Engineering in Medicine and Biology Society, 2011, 4499-4502. <https://doi.org/10.1109/IEMBS.2011.6091115>
34. Rilling J. K., Seligman, R. A. A Quantitative Morphometric Comparative Analysis of the Primate Temporal Lobe. *Journal of Human Evolution*, 2002, 42(5), 505-533. <https://doi.org/10.1006/jhev.2001.0537>
35. Schouten, T. M., et al. Combining Anatomical, Diffusion, and Resting State Functional Magnetic Resonance Imaging for Individual Classification of Mild and Moderate Alzheimer's Disease. *NeuroImage: Clinical*, 2016, 11, 46-51. <https://doi.org/10.1016/j.nicl.2016.01.002>
36. Shankar, K., Lakshmana, Prabhu, S. K., Khanna, A., Tanwar, S., Joel, J., Rodrigues, P. C., Roy, N. R. Alzheimer Detection Using Group Grey Wolf Optimization Based Features with Convolutional Classifier. *Computers & Electrical Engineering*, 2019, 77, 230-243. <https://doi.org/10.1016/j.compeleceng.2019.06.001>
37. Vemuri, P., Gunter, J. L., Senjem, M. L., Whitwell, J. L., Kantarci, K., Knopman, D. S., Boeve, B. F., Petersen, R. C., Jack Jr, C. R. Alzheimer's Disease Diagnosis in Individual Subjects Using Structural MR Images: Validation Studies. *Neuroimage*, 2008, 39(3), 1186-1197. <https://doi.org/10.1016/j.neuroimage.2007.09.073>
38. Vos, F. D., Schouten, T. M., Hafkemeijer, A., Dopper, E. G., van Swieten, J. C., de Rooij, M., van der Grond, J., Rombouts, S. A. Combining Multiple Anatomical MRI Measures Improves Alzheimer's Disease Classification. *Human Brain Mapping*, 2016, 37(5), 1920-1929. <https://doi.org/10.1002/hbm.23147>
39. Wang, S. H., Phillips, P., Sui, Y., Liu, B., Yang, M., Cheng, H. Classification of Alzheimer's Disease Based on Eight-Layer Convolutional Neural Network with Leaky Rectified Linear Unit and Max Pooling. *Journal of Medical Systems*, 2018, 42(5), 85. <https://doi.org/10.1007/s10916-018-0932-7>
40. Xu, Y., Jack, C. R., O'Brien, P. C., Kokmen, E., Smith, G. E., Ivnik, R. J., Bove, B. F., Tangalos, R. G., Petersen, R. C. Usefulness of MRI Measures of Entorhinal Cortex Versus Hippocampus in AD. *Neurology*, 2000, 54(9), 1760-1767. <https://doi.org/10.1212/WNL.54.9.1760>
41. Yadav, G., Maheshwari, S., Agarwal, A. Contrast Limited Adaptive Histogram Equalization Based Enhancement for Real Time Video System. *Proceedings of the 2014 International Conference on Advances in Computing, Communications and Informatics, ICACCI 2014*, 2014, 2392-2397. <https://doi.org/10.1109/ICACCI.2014.6968381>
42. Zhang, Y., Wang, S., Dong, Z. Classification of Alzheimer Disease Based on Structural Magnetic Resonance Imaging by Kernel Support Vector Machine Decision Tree. *Progress in Electromagnetics Research*, 2014, 144, 171-184. <https://doi.org/10.2528/PIER13121310>
43. Zhang, B., Allebach, J. P. Adaptive Bilateral Filter for Sharpness Enhancement and Noise Removal. *IEEE Transactions on Image Processing*, 2008, 17(5), 664-678. <https://doi.org/10.1109/TIP.2008.919949>
44. Zhang, X., Cui, J., Wang, W., Lin, C. A Study for Texture Feature Extraction of High-Resolution Satellite Images Based on a Direction Measure and Gray Level Co-Occurrence Matrix Fusion Algorithm. *Sensors (Switzerland)*, 2017, 17(7). <https://doi.org/10.3390/s17071474>

